Letter

Dynamical signatures of symmetry-broken and liquid phases in an $S = \frac{1}{2}$ Heisenberg antiferromagnet on the triangular lattice

Markus Drescher,[1,*] Laurens Vanderstraeten,[2] Roderich Moessner,[3] and Frank Pollmann[1,4]
[1]*Department of Physics, Technische Universität München, 85748 Garching, Germany*
[2]*Center for Nonlinear Phenomena and Complex Systems, Université Libre de Bruxelles, 1050 Brussels, Belgium*
[3]*Max-Planck-Institut für Physik komplexer Systeme, 01187 Dresden, Germany*
[4]*Munich Center for Quantum Science and Technology (MCQST), 80799 Munich, Germany*

(Received 17 September 2022; revised 24 July 2023; accepted 2 November 2023; published 5 December 2023)

We present the dynamical spin structure factor of the antiferromagnetic spin-$\frac{1}{2}$ J_1-J_2 Heisenberg model on a triangular lattice obtained from large-scale matrix-product state simulations. The high frustration due to the combination of antiferromagnetic nearest- and next-nearest-neighbor interactions yields a rich phase diagram. We resolve the low-energy excitations both in the 120° ordered phase and in the putative spin-liquid phase at $J_2/J_1 = 0.125$. In the ordered phase, we observe an avoided decay of the lowest magnon branch, demonstrating the robustness of this phenomenon in the presence of gapless excitations. Our findings in the spin-liquid phase chime with the field-theoretical predictions for a gapless Dirac spin liquid, in particular the picture of low-lying monopole excitations at the corners of the Brillouin zone. We comment on possible practical difficulties of distinguishing proximate liquid and solid phases based on the dynamical structure factor.

DOI: 10.1103/PhysRevB.108.L220401

Introduction.—Quantum spin liquids (QSLs) [1–4] are exotic, entangled phases of matter characterized by a lack of magnetic order at zero temperature and the emergence of fractionalized quasiparticle excitations. They have received substantial attention both in theory and experiment, giving rise to various proposals regarding the nature of the candidate QSL phases on frustrated spin systems [5–24]. Using state-of-the-art numerics, we study the paradigmatic antiferromagnetic J_1-J_2 Heisenberg Hamiltonian on a triangular lattice (TLHAF)

$$H = J_1 \sum_{\langle i,j \rangle} \hat{\mathbf{S}}_i \cdot \hat{\mathbf{S}}_j + J_2 \sum_{\langle\langle i,j \rangle\rangle} \hat{\mathbf{S}}_i \cdot \hat{\mathbf{S}}_j, \tag{1}$$

where $\langle i, j\rangle$ and $\langle\langle i, j\rangle\rangle$ denote pairs of nearest-neighbor and next-nearest-neighbor sites, respectively, thereby aiming to find dynamical fingerprints of the distinct phases that have been proposed theoretically.

Following Anderson's original proposal [25] that the ground state of the nearest-neighbor TLHAF could stabilize a resonating valence bond state, there have been intense investigations into the nature of quantum spin models on the frustrated geometry of the triangular lattice [16,17,26,27]. Even though the ground state for the nearest-neighbor model has been established to have a coplanar 120° Néel order [28–32], the underlying geometry still provides one of the simplest cases for the emergence of a QSL phase [33]. Adding a next-nearest-neighbor coupling J_2, there is classically a phase transition at $\frac{J_2}{J_1} = \frac{1}{8}$ between the 120° Néel order and a four-sublattice ordered phase with a residual degeneracy [33–35]. For the quantum model, however, numerical simulations indicate a QSL phase around the point of the classical phase transition for $0.07 \lesssim \frac{J_2}{J_1} \lesssim 0.15$, the nature of which has been under debate [16–20,22,23,26,36,37]. It is followed by a collinear stripe-ordered phase for larger J_2 [16,26,33] (cf. Fig. 1). Despite recent progress in the quest for candidate materials [18,45,46], most promisingly with respect to rare-earth delafossites [21,47–49], the unambiguous detection of a QSL remains an open issue, with only very recent encouraging reports [24].

From a theoretical perspective, the computation of spectral functions of two-dimensional quantum magnets has been a challenge as well, triggering work in analytical techniques [30–32,50–54], variational Monte Carlo simulations [20,55], and tensor-network approaches [56–59]. Using large-scale matrix-product state (MPS) methods [60–64], we compute the dynamical correlations of the system both in the ordered 120° phase for $J_2 = 0$ and the adjacent candidate QSL phase at $\frac{J_2}{J_1} = 0.125$, which allows us to compute the spectral function of the model. We complement these time-evolution calculations by applying the quasiparticle ansatz, a variational approach for targeting excited states on top of a given MPS ground state for the infinite cylinder directly [65,66].

Our central insights are the following. First, we find that the magnon mode in the ordered phase of the *isotropic* model is stable even when kinematically its decay is allowed. The mechanism, termed avoided quasiparticle decay, had been reported for a TLHAF with an easy-axis anisotropy [67] but its stability in the presence of gapless excitations had remained in question. Second, we investigate the dynamical features of the spectral function in the candidate QSL, and compare these to those of the ordered phase. The outstanding agreement between the time evolution and the quasiparticle ansatz suggests that both can be used as complementary methods. In the candidate QSL phase, we find prominent low-energy excitations at the corners of the Brillouin zone, in agreement with the field-theoretical prediction of triplet monopole exci-

*markus.drescher@tum.de

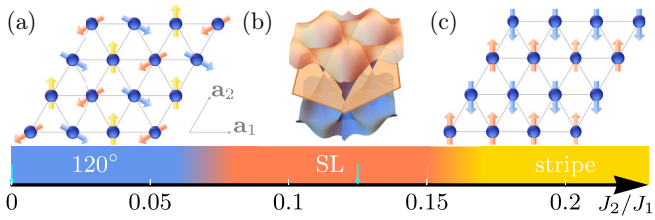

FIG. 1. Phase diagram of the J_1-J_2 antiferromagnetic Heisenberg model on a triangular lattice. At the Heisenberg point $J_2 = 0$, the ground state exhibits a 120° order (a). Around $\frac{J_2}{J_1} \approx 0.07$, there is a transition into a candidate quantum spin-liquid state (b). In the illustration, we show the dispersion of the spinons at half-filling in the mean-field solution of the Dirac spin liquid discussed in Sec. F in the Supplemental Material [38]. For larger next-nearest-neighbor couplings, a stripe-ordered phase emerges (c). The blue arrows at $J_2 = 0$ and $\frac{J_2}{J_1} = 0.125$ denote the points in the different regimes where we compute the spectral function.

tations in a $U(1)$ Dirac spin liquid (DSL) [68–70], suggesting important gauge fluctuations within the parton construction of the DSL.

Numerical Methods.—We use large-scale MPS simulations to find the ground state and the excitation spectrum of the J_1-J_2 TLHAF in two different regimes indicated in Fig. 1. The triangular lattice is wrapped onto a cylindrical geometry with periodic boundary conditions along the circumference L_y [56,71]. We consider a YC6-0 geometry [19,26], where $L_y = 6$ specifies the circumference of the cylinder and $n = 0$ determines the boundary condition by identifying sites $\mathbf{r}$ and $\mathbf{r} + L_y\,\mathbf{a}_2 - n\,\mathbf{a}_1$ with $\mathbf{a}_{1/2}$ being the primitive vectors of the Bravais lattice [Fig. 1(a)]. We find an MPS ground-state approximation using either the infinite DMRG [72–74] or the VUMPS algorithm [64,75]. From this infinite ground-state MPS, the static spin structure factor

$$\chi(\mathbf{k}) = \frac{1}{N}\sum_{i,j} e^{-\mathrm{i}\mathbf{k}\cdot(\mathbf{r}_i - \mathbf{r}_j)}\,\langle \hat{\mathbf{S}}_i \cdot \hat{\mathbf{S}}_j \rangle \tag{2}$$

can be readily obtained as shown in Fig. 2.

We compute the dynamical spin structure factor—or spectral function—from the time-resolved spatial spin-spin correlations of the system

$$S^{+-}(\mathbf{k},\omega) = \int \mathrm{d}t \sum_j e^{\mathrm{i}\omega t - \mathrm{i}\mathbf{k}\cdot(\mathbf{r}_j - \mathbf{r}_{j_c})}\,\langle \hat{S}^+_j(t)\hat{S}^-_{j_c}(0)\rangle\,, \tag{3}$$

where j_c denotes the center site of the lattice and $\hat{S}^{\pm}_j = \hat{S}^x_j \pm \mathrm{i}\hat{S}^y_j$ are the spin ladder operators. The simulations are performed on long cylinders of dimension $L_y \times L_x$. Depending on the parameter regime, we have used $L_x = 51$ or $L_x = 126$. The dynamical correlations are obtained by applying a local operator $\hat{S}^-_{j_c}$ at the center of the system and time-evolving the perturbed ground state using the MPO W_{II} time-evolution algorithm for MPS with long-range interactions [62,63]. For a time step size of $\delta t = 0.04\,J_1$, we measured the correlations $C^{+-}_{i,j_c}(t) \equiv \langle \hat{S}^+_i(t)\hat{S}^-_{j_c}\rangle$ every $N_{\mathrm{steps}} = 5$ time steps. We obtain the spectral function by taking the momentum superposition of $C^{+-}_{i,j_c}(t)$, and transforming to frequency space by a numerical integration with a Gaussian envelope and linear-prediction techniques [76]. The Gaussian window function thereby ensures that the actual simulation data has a large weight whereas the predicted data lie in its tail with the main purpose of suppressing Gibb's oscillations in the Fourier signal (see Sec. A in the Supplemental Material [38] for further details). The entanglement entropy in the state is expected to grow under unitary time evolution, increasing the difficulty to faithfully represent the quantum state. Hence, the total time that we can access in our simulations is limited by the bond dimension of the MPS. We have used bond dimensions up to $\chi = 1500$ in the ordered and $\chi = 2000$ in the QSL phase with a total simulation time up to $60\,J_1$ and have made sure that the system is large enough in order to avoid boundary artifacts. Moreover, we have applied operators with defined k_y momentum instead of single-site operators to better resolve the gapless K points (see also Sec. A in the Supplemental Material [38]).

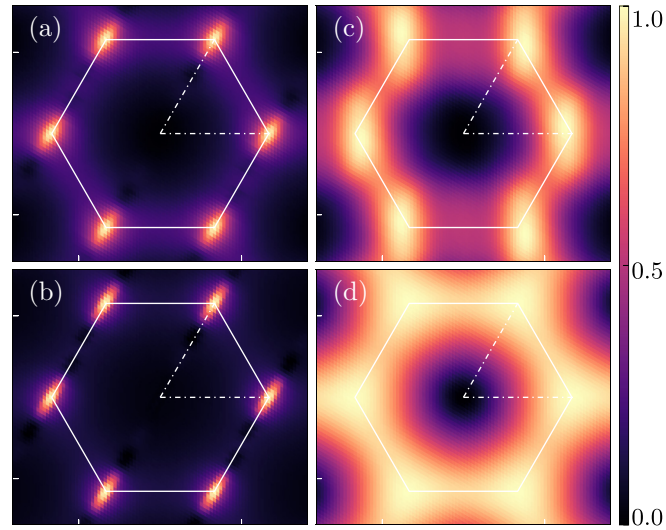

FIG. 2. Comparison of the static spin structure factor $\chi(\mathbf{k})$ on a cylinder with $L_y = 6$ from numerical DMRG results (top row) and analytical calculations (bottom row). (a) DMRG result for the 120° ordered phase at $J_2 = 0$ and (b) the corresponding linear spin-wave theory. A cubic interpolation scheme along the circumference has been used for plotting. The right column shows the static structure factor in the QSL phase at $\frac{J_2}{J_1} = 0.125$ for (c) DMRG and (d) the analytic result from the Dirac spin-liquid parton theory. The cylinder geometry used is 6×51 for panels (a)–(c) and 6×50 for (d).

We next compare these results to those obtained by the variational quasiparticle ansatz [65,66]. Compared to the time evolution, this variational approach involves a numerically cheaper calculation, and provides a good approximation to the energy of the lowest-lying excited state at a certain momentum $\mathbf{k}$. As such, it provides the dispersion of isolated modes in the spectrum or the lower edges of continua. In addition, using the variational wavefunctions for the lowest-lying excitations, we can compute the spectral weights and obtain their contribution to the spectral function in the Lehmann representation [77].

120° *Ordered Phase.*—The static structure factor $\chi(\mathbf{k})$ exhibits characteristics of the 120° coplanar Néel order of the ground state at the Heisenberg point $J_2 = 0$ via the well-pronounced maxima at the corners of the Brillouin

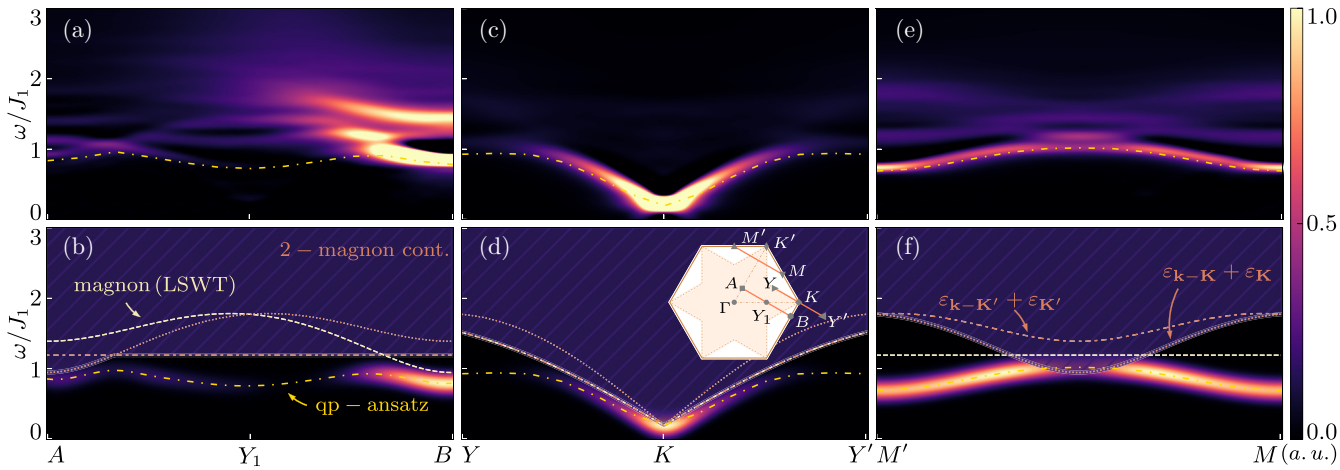

FIG. 3. Upper row: The spectral function in the ordered phase with only nearest-neighbor coupling ($J_2 = 0$) along different paths in the Brillouin zone as indicated in the inset in (d). The golden dot-dashed line shows the result for the lowest-excitation energy obtained from the quasiparticle ansatz. Lower row: Results from linear spin-wave theory (LSWT) to be compared to the MPS data in the panels above. The dashed bright line denotes the single-magnon branch. The red dotted line shows the minimum of the two-magnon continuum at $\mathbf{q} = \mathbf{K}$, whereas the red dot-dashed line corresponds to the local minimum for $\mathbf{q} = \mathbf{K}'$. The resulting two-magnon continuum is given by the hatched area. We indicate again the lowest-energy mode obtained from the quasiparticle ansatz and plot it additionally with a Gaussian broadening of $\sigma = 0.1$ and weighted with the corresponding spectral weights (cf. Sec. B in the Supplemental Material [38]). Note that the finite-size gap determined at K from the quasiparticle ansatz has been taken as an energy offset for the linear spin-wave results. We used system sizes 6×126 and bond dimensions up to $\chi = 1500$.

zone K, K' and related points shown in Fig. 2. Comparing with the results from linear spin-wave theory (LSWT), where the classical three-sublattice 120° order is weakened by quantum fluctuations (see Sec. E in the Supplemental Material [38] for details of the calculation), we find conclusive agreement.

Figure 3 shows the results for the spectral function from the MPS simulations for $J_2 = 0$. Previous investigations of the low-energy excitations of the ordered phase beyond LSWT using semiclassical approaches such as higher-order spin-wave theory [29,31,32] or series expansions [51,52] already obtained strong renormalizations of the magnon dispersion mainly caused by interactions between the single quasiparticle branches and the magnon continuum. One prominent feature is a pronounced rotonlike minimum at the M point and symmetry-related points (the centers of the edges of the Brillouin zone). Our numerics confirms this characteristic as shown in Fig. 3(e). The spectral weight is concentrated at the M points in a smaller frequency window, leading to a distinct maximum in the intensity although the integrated spectral weight of the lowest branch exhibits a local minimum (cf. Sec. C in the Supplemental Material [38]). Using the quasiparticle ansatz, we find good agreement for the overall spectral weight of the lowest renormalized magnon branch. The energy dispersion from this ansatz with the associated spectral weight displayed as a Gaussian broadening of $\sigma = 0.1$ is plotted in Fig. 3(f). The bright dashed line denotes the magnon branch from LSWT. We observe a strong downward renormalization that is consistent with previous findings [32,50]. The lower bound of the two-magnon continuum is given by the minimum of the decays $\varepsilon_{\mathbf{k}} = \varepsilon_{\mathbf{k}-\mathbf{q}} + \varepsilon_{\mathbf{q}}$ with $\mathbf{q} = \mathbf{K}$ and $\mathbf{q} = \mathbf{K}'$ [32]. Both dispersions are schematically shown in Fig. 3(f). In our simulations on an $L_y = 6$ cylinder, the spectral weight distribution above the isolated lowest mode in Fig. 3(e) exhibits features of both decay channels and the noninteracting magnon line alongside some distortions around the touching points. It remains an open question if this is a finite-size effect or whether it survives in the thermodynamic limit.

A rotonlike minimum, however, does not only occur at the M points, but also at Y_1, the midpoint between A and B [cf. inset Fig. 3(d)]. This was first suggested by Verresen *et al.* [67] in the case of an antiferromagnetic triangular Heisenberg model with a small anisotropic term that makes it numerically more tractable by slightly gapping out the Goldstone modes. Moreover, also variational Monte Carlo simulations [20] have found a similar feature that can be associated with avoided quasiparticle decay due to strong interactions between the lowest mode and the two-magnon continuum [67]. Fig. 3(a) shows the spectral function of the pure Heisenberg model on the triangular lattice along the cut $A - B$. Besides a pronounced maximum at B and a diffuse continuum reaching up to energies of roughly $3J_1$, we again observe remnants of the single-magnon mode and the decay channels representing the minima of the energy surface described by the lower boundary of the two-magnon continuum. The lowest-energy mode, however, stays beneath the onset of the continuum, supporting the previous conjecture that avoided magnon-decay is a valid feature of the theory [20,67]. The variation of the integrated spectral weight of the repelled magnon mode is confirmed within the quasiparticle ansatz (see Sec. C in the Supplemental Material [38]).

The Goldstone modes at the corners of the Brillouin zone K and K' exhibit a high concentration of spectral weight [Fig. 3(c)]. This agrees with previous numerical and experimental findings [20,21,78]. Due to finite-size effects, the magnon modes develop a gap. The corresponding gap determined at K for the quasiparticle ansatz has been taken as a

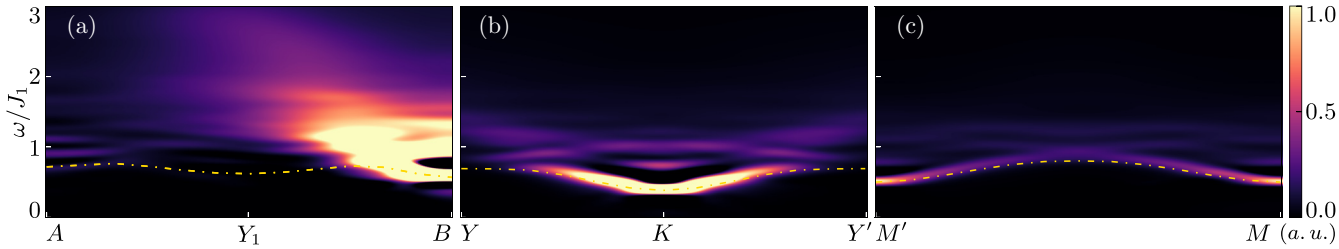

FIG. 4. Spectral function in the candidate QSL phase at $\frac{J_2}{J_1} = 0.125$ along the same momentum cuts as in Fig. 3 obtained on a cylinder geometry with $L_y = 6$ and $L_x = 51$. The dot-dashed line denotes the corresponding lowest-energy mode from the quasiparticle ansatz. We used bond dimension $\chi = 2000$ for these simulations.

reference offset when plotting the analytic linear spin-wave results in Fig. 3.

Stripe-Ordered Phase.—For $\frac{J_2}{J_1} \gtrsim 0.15$, we obtain a stripe-ordered phase. The DMRG algorithm applied here for the ground-state optimization chooses a certain symmetry-broken state as the ground state. As a result, the static structure factor displays a peak at M', but not at M. In accordance with analytical expectations, we observe a gapless Goldstone mode at M'. Plots of the spectral function for $\frac{J_2}{J_1} = 0.55$ deep in the symmetry-broken phase are provided in Sec. D in the Supplemental Material [38]. We observe clear magnon modes in good agreement with the predictions from linear spin-wave theory.

From pure LSWT, however, we expect accidental zero modes at the edge centers of the Brillouin zone where no Goldstone mode resides. In contrast, our results suggest a clear finite gap that exceeds the finite-size gap of the system (cf. Sec. D in the Supplemental Material [38] for details). This is in line with the established understanding that quantum fluctuations in the Heisenberg model gap out the accidental zero modes [34,35,79].

Candidate QSL Phase.—While the existence of a QSL phase around the classical phase transition point $\frac{J_2}{J_1} = 0.125$ is rather well-established, the precise nature of this phase is highly debated so far, reaching from gapped Z_2 spin liquids to gapless $U(1)$ Dirac spin liquids (DSL) or chiral spin liquids [17,20,26]. Note that the J_1-J_2 triangular Heisenberg model on an even cylinder comprises two different topological sectors in the candidate QSL phase [16,26]. The sector of the isotropic ground state can be reached by adiabatically inserting a flux $\theta = 2\pi$ [19] (cf. Sec. A in the Supplemental Material [38] for further details). We focus on this sector for our simulations and all subsequent results.

Figure 4 shows the dynamical structure factor for $\frac{J_2}{J_1} = 0.125$. We observe a softening of the minima at the M points compared to the ordered phase, which can be attributed to the existence of spinon bilinears at the centers of the edges [69] in a $U(1)$ DSL. Apart from this, the continuum is shifted downwards with varying strength between M' and M, diminishing the distance in energy between the lowest-energy mode and the onset of the continuum. This is in accordance with variational Monte Carlo data that suggests a vanishing separation of the continuum from lowest-energy excitations in the QSL phase [20]. Even though we expect the bilinear excitations to become gapless in the two-dimensional limit (i.e., $L_y \to \infty$), we observe a clear gap in the spectral function. This can be related to the geometry of the $L_y = 6$ cylinder: The accessible momenta do not include the spinon Dirac cones at $\pm\mathbf{Q} = \pm(\frac{\pi}{2}, \frac{\pi}{2\sqrt{3}})$ [80] (see Sec. G in the Supplemental Material [38]), which gaps out the corresponding spectral function. The spectral maximum at B survives across the transition from the ordered phase to the QSL phase [Fig. 4(a)] as well as the feature of the lowest mode with almost vanishing weight being repelled from the continuum at intermediate energies [Fig. 4(a)]—although the spectral function shows different distinct modes below the more pronounced continuum.

Perhaps the most striking aspect, however, is the structure of the excitations at the K points. As for the Goldstone mode in the symmetry-broken phase, there is a minimum in the candidate QSL phase, albeit with a flatter dispersion and a rich structure of the distribution of the spectral weight above the minimum in contrast to the 120° phase. The locations of the minima at K and K' and related points are in accordance with the field-theoretical predictions by Song *et al.* [69,70]: They report the occurrence of triplet monopole excitations at the corners of the Brillouin zone for a $U(1)$ DSL on a triangular lattice. The comparison of Fig. 4(b) with variational Monte Carlo data for a DSL ansatz [20,81] supports this conjecture. At the transition to the ordered phase for smaller J_2 coupling, the monopole operators whose quantum numbers correspond to the K points condense [69,82], thus building up the familiar three-sublattice order. The comparison of the static structure factor sustains this theory: Although in the QSL phase at $\frac{J_2}{J_1} = 0.125$, $\chi(\mathbf{k})$ still exhibits maxima in the intensity around the K points of the Brillouin zone (Fig. 2), the structure factor obtained from DMRG simulations has a much broader and more diffuse structure than in the ordered phase at $J_2 = 0$, which compares well with the analytic result for a $U(1)$ DSL [Fig. 2(d)], suggesting qualitative agreement notwithstanding the finite-cylinder effects.

Conclusions.—We have studied the dynamical properties of ordered and candidate spin-liquid phases in the triangular lattice. We find excellent agreement between the time evolution and the quasiparticle ansatz. In the ordered phase, we observe the avoided decay of the lowest magnon branch previously shown to occur in an anisotropic Heisenberg model [67]. In the candidate QSL phase, our numerical MPS results for the Heisenberg model on a cylinder show good agreement with the results obtained from variational Monte Carlo simulations [20], where the gapless $U(1)$ Dirac spin-liquid nature of the ground state is assumed. Given that the method we apply does not depend on any previous knowledge or assumptions on the

wave function of the ground state, this validates the variational $U(1)$ DSL approach.

In closing, we would like to make the following observation. While the responses of the two phases can be visually quite distinct, see, e.g., the broad features in the QSL in Fig. 2, the differences are perhaps overall less striking than one might have hoped for. Indeed, inspecting Figs. 3 and 4 yields copious similarities between the two dynamical structure factors. This underlines the challenge inherent in discriminating proximate phases whose universal low-energy physics may be fundamentally distinct, but which may nonetheless harbor similar finite-time and short-distance correlations. Of course, if a reliably determined microscopic Hamiltonian for a material under consideration is available, our microscopic approach can be used for a direct *quantitative* validation of the correspondence between experimental results and theoretical interpretation. Absent this, it may very well be possible to account for salient finite-time and short-distance correlations from different starting points. That this should be the case of course is what makes the universal response so special by contrast; but in practice, this can pose a formidable challenge in the interpretation of experimental data.

Note added.—While finalizing the current draft, we became aware of a similar work about the spectral function of different phases on the TLHAF [83].

Acknowledgments.—We would like to thank Ruben Verresen, Wilhelm Kadow and Johannes Knolle for helpful discussions and Francesco Ferrari and Federico Becca for providing additional data for spectral functions from variational Monte Carlo simulations. F.P. acknowledges support of the European Research Council (ERC) under the European Union's Horizon 2020 research and innovation program (Grant No. 771537). F.P. also acknowledges the support of the Deutsche Forschungsgemeinschaft (DFG, German Research Foundation) under Germany's Excellence Strategy Grant No. EXC-2111-390814868. F.P.'s research is part of the Munich Quantum Valley, which is supported by the Bavarian state government with funds from the Hightech Agenda Bayern Plus. This work was in part supported by the Deutsche Forschungsgemeinschaft under Grant No. SFB 1143 (Project No. 247310070) and cluster of excellence ct.qmat (EXC 2147, Project No. 390858490). L.V. is supported by the Research Foundation Flanders (FWO) via Grant No. FWO20/PDS/115.

[1] X.-G. Wen, Phys. Rev. B **65**, 165113 (2002).
[2] L. Balents, Nature (London) **464**, 199 (2010).
[3] L. Savary and L. Balents, Rep. Prog. Phys. **80**, 016502 (2017).
[4] J. Knolle and R. Moessner, Annu. Rev. Condens. Matter Phys. **10**, 451 (2019).
[5] A. Kitaev, Ann. Phys. **321**, 2 (2006), january Special Issue.
[6] J. Knolle, D. L. Kovrizhin, J. T. Chalker, and R. Moessner, Phys. Rev. B **92**, 115127 (2015).
[7] K. Kitagawa, T. Takayama, Y. Matsumoto, A. Kato, R. Takano, Y. Kishimoto, S. Bette, R. Dinnebier, G. Jackeli, and H. Takagi, Nature (London) **554**, 341 (2018).
[8] H. Takagi, T. Takayama, G. Jackeli, G. Khaliullin, and S. E. Nagler, Nat. Rev. Phys. **1**, 264 (2019).
[9] S. Sachdev, Phys. Rev. B **45**, 12377 (1992).
[10] M. B. Hastings, Phys. Rev. B **63**, 014413 (2000).
[11] Y. Ran, M. Hermele, P. A. Lee, and X.-G. Wen, Phys. Rev. Lett. **98**, 117205 (2007).
[12] Y. Iqbal, D. Poilblanc, and F. Becca, Phys. Rev. B **91**, 020402 (2015).
[13] Y.-C. He, M. P. Zaletel, M. Oshikawa, and F. Pollmann, Phys. Rev. X **7**, 031020 (2017).
[14] H. J. Liao, Z. Y. Xie, J. Chen, Z. Y. Liu, H. D. Xie, R. Z. Huang, B. Normand, and T. Xiang, Phys. Rev. Lett. **118**, 137202 (2017).
[15] M. Fujihala, K. Morita, R. Mole, S. Mitsuda, T. Tohyama, S.-i. Yano, D. Yu, S. Sota, T. Kuwai, A. Koda, H. Okabe, H. Lee, S. Itoh, T. Hawai, T. Masuda, H. Sagayama, A. Matsuo, K. Kindo, S. Ohira-Kawamura, and K. Nakajima, Nat. Commun. **11**, 3429 (2020).
[16] W.-J. Hu, S.-S. Gong, W. Zhu, and D. N. Sheng, Phys. Rev. B **92**, 140403 (2015).
[17] Y. Iqbal, W.-J. Hu, R. Thomale, D. Poilblanc, and F. Becca, Phys. Rev. B **93**, 144411 (2016).
[18] Y. Shen, Y.-D. Li, H. Wo, Y. Li, S. Shen, B. Pan, Q. Wang, H. C. Walker, P. Steffens, M. Boehm, Y. Hao, D. L. Quintero-Castro, L. W. Harriger, M. D. Frontzek, L. Hao, S. Meng, Q. Zhang, G. Chen, and J. Zhao, Nature (London) **540**, 559 (2016).
[19] S. Hu, W. Zhu, S. Eggert, and Y.-C. He, Phys. Rev. Lett. **123**, 207203 (2019).
[20] F. Ferrari and F. Becca, Phys. Rev. X **9**, 031026 (2019).
[21] A. O. Scheie, E. A. Ghioldi, J. Xing, J. A. M. Paddison, N. E. Sherman, M. Dupont, L. D. Sanjeewa, S. Lee, A. J. Woods, D. Abernathy, D. M. Pajerowski, T. J. Williams, S.-S. Zhang, L. O. Manuel, A. E. Trumper, C. D. Pemmaraju, A. S. Sefat, D. S. Parker, T. P. Devereaux, R. Movshovich, J. E. Moore, C. D. Batista, and D. A. Tennant, Nat. Phys. (2023), doi:10.1038/s41567-023-02259-1.
[22] Y.-F. Jiang and H.-C. Jiang, Phys. Rev. B **107**, L140411 (2023).
[23] T. Tang, B. Moritz, and T. P. Devereaux, Phys. Rev. B **106**, 064428 (2022).
[24] S. Xu, R. Bag, N. E. Sherman, L. Yadav, A. I. Kolesnikov, A. A. Podlesnyak, J. E. Moore, and S. Haravifard, arXiv:2305.20040 [cond-mat.str-el].
[25] P. Anderson, Mater. Res. Bull. **8**, 153 (1973).
[26] Z. Zhu and S. R. White, Phys. Rev. B **92**, 041105 (2015).
[27] S. N. Saadatmand and I. P. McCulloch, Phys. Rev. B **94**, 121111 (2016).
[28] B. Bernu, P. Lecheminant, C. Lhuillier, and L. Pierre, Phys. Rev. B **50**, 10048 (1994).
[29] L. Capriotti, A. E. Trumper, and S. Sorella, Phys. Rev. Lett. **82**, 3899 (1999).
[30] A. L. Chernyshev and M. E. Zhitomirsky, Phys. Rev. Lett. **97**, 207202 (2006).

[31] O. A. Starykh, A. V. Chubukov, and A. G. Abanov, Phys. Rev. B **74**, 180403 (2006).
[32] A. L. Chernyshev and M. E. Zhitomirsky, Phys. Rev. B **79**, 144416 (2009).
[33] Z. Zhu, P. A. Maksimov, S. R. White, and A. L. Chernyshev, Phys. Rev. Lett. **120**, 207203 (2018).
[34] T. Jolicoeur, E. Dagotto, E. Gagliano, and S. Bacci, Phys. Rev. B **42**, 4800 (1990).
[35] A. V. Chubukov and T. Jolicoeur, Phys. Rev. B **46**, 11137 (1992).
[36] R. Kaneko, S. Morita, and M. Imada, J. Phys. Soc. Jpn. **83**, 093707 (2014).
[37] S.-S. Gong, W. Zheng, M. Lee, Y.-M. Lu, and D. N. Sheng, Phys. Rev. B **100**, 241111 (2019).
[38] See Supplemental Material at http://link.aps.org/supplemental/10.1103/PhysRevB.108.L220401 for details on the numerical computations, spin-wave theory and the mean-field theory for the Dirac spin liquid, which includes Refs. [39–44].
[39] P. W. Anderson, Phys. Rev. **86**, 694 (1952).
[40] R. Kubo, Phys. Rev. **87**, 568 (1952).
[41] S. Singh, R. N. C. Pfeifer, and G. Vidal, Phys. Rev. A **82**, 050301 (2010).
[42] S. Singh, R. N. C. Pfeifer, and G. Vidal, Phys. Rev. B **83**, 115125 (2011).
[43] R. Deutscher and H.-U. Everts, Z. Phys. B **93**, 77 (1993).
[44] A. E. Trumper, L. Capriotti, and S. Sorella, Phys. Rev. B **61**, 11529 (2000).
[45] Y. Shen, Y.-D. Li, H. C. Walker, P. Steffens, M. Boehm, X. Zhang, S. Shen, H. Wo, G. Chen, and J. Zhao, Nat. Commun. **9**, 4138 (2018).
[46] W. Ruan, Y. Chen, S. Tang, J. Hwang, H.-Z. Tsai, R. L. Lee, M. Wu, H. Ryu, S. Kahn, F. Liou, C. Jia, A. Aikawa, C. Hwang, F. Wang, Y. Choi, S. G. Louie, P. A. Lee, Z.-X. Shen, S.-K. Mo, and M. F. Crommie, Nat. Phys. **17**, 1154 (2021).
[47] M. M. Bordelon, E. Kenney, C. Liu, T. Hogan, L. Posthuma, M. Kavand, Y. Lyu, M. Sherwin, N. P. Butch, C. Brown, M. J. Graf, L. Balents, and S. D. Wilson, Nat. Phys. **15**, 1058 (2019).
[48] R. Sarkar, P. Schlender, V. Grinenko, E. Haeussler, P. J. Baker, T. Doert, and H.-H. Klauss, Phys. Rev. B **100**, 241116 (2019).
[49] P.-L. Dai, G. Zhang, Y. Xie, C. Duan, Y. Gao, Z. Zhu, E. Feng, Z. Tao, C.-L. Huang, H. Cao, A. Podlesnyak, G. E. Granroth, M. S. Everett, J. C. Neuefeind, D. Voneshen, S. Wang, G. Tan, E. Morosan, X. Wang, H.-Q. Lin *et al.*, Phys. Rev. X **11**, 021044 (2021).
[50] M. Mourigal, W. T. Fuhrman, A. L. Chernyshev, and M. E. Zhitomirsky, Phys. Rev. B **88**, 094407 (2013).
[51] W. Zheng, J. O. Fjærestad, R. R. P. Singh, R. H. McKenzie, and R. Coldea, Phys. Rev. B **74**, 224420 (2006).
[52] W. Zheng, J. O. Fjærestad, R. R. P. Singh, R. H. McKenzie, and R. Coldea, Phys. Rev. Lett. **96**, 057201 (2006).
[53] E. A. Ghioldi, M. G. Gonzalez, S.-S. Zhang, Y. Kamiya, L. O. Manuel, A. E. Trumper, and C. D. Batista, Phys. Rev. B **98**, 184403 (2018).
[54] E. A. Ghioldi, S.-S. Zhang, Y. Kamiya, L. O. Manuel, A. E. Trumper, and C. D. Batista, Phys. Rev. B **106**, 064418 (2022).
[55] F. Ferrari and F. Becca, Phys. Rev. B **98**, 100405 (2018).
[56] M. Gohlke, R. Verresen, R. Moessner, and F. Pollmann, Phys. Rev. Lett. **119**, 157203 (2017).
[57] R. Verresen, F. Pollmann, and R. Moessner, Phys. Rev. B **98**, 155102 (2018).
[58] R. Chi, Y. Liu, Y. Wan, H.-J. Liao, and T. Xiang, Phys. Rev. Lett. **129**, 227201 (2022).
[59] W. Kadow, L. Vanderstraeten, and M. Knap, Phys. Rev. B **106**, 094417 (2022).
[60] U. Schollwöck, Ann. Phys. **326**, 96 (2011).
[61] J. Hauschild and F. Pollmann, SciPost Phys. Lect. Notes **5** (2018).
[62] M. P. Zaletel, R. S. K. Mong, C. Karrasch, J. E. Moore, and F. Pollmann, Phys. Rev. B **91**, 165112 (2015).
[63] S. Paeckel, T. Köhler, A. Swoboda, S. R. Manmana, U. Schollwöck, and C. Hubig, Ann. Phys. **411**, 167998 (2019).
[64] L. Vanderstraeten, J. Haegeman, and F. Verstraete, SciPost Phys. Lect. Notes **7** (2019).
[65] J. Haegeman, B. Pirvu, D. J. Weir, J. I. Cirac, T. J. Osborne, H. Verschelde, and F. Verstraete, Phys. Rev. B **85**, 100408 (2012).
[66] M. Van Damme, R. Vanhove, J. Haegeman, F. Verstraete, and L. Vanderstraeten, Phys. Rev. B **104**, 115142 (2021).
[67] R. Verresen, R. Moessner, and F. Pollmann, Nat. Phys. **15**, 750 (2019).
[68] M. Hermele, T. Senthil, and M. P. A. Fisher, Phys. Rev. B **72**, 104404 (2005).
[69] X.-Y. Song, C. Wang, A. Vishwanath, and Y.-C. He, Nat. Commun. **10**, 4254 (2019).
[70] X.-Y. Song, Y.-C. He, A. Vishwanath, and C. Wang, Phys. Rev. X **10**, 011033 (2020).
[71] E. Stoudenmire and S. R. White, Annu. Rev. Condens. Matter Phys. **3**, 111 (2012).
[72] S. R. White, Phys. Rev. Lett. **69**, 2863 (1992).
[73] S. R. White, Phys. Rev. B **48**, 10345 (1993).
[74] I. P. McCulloch, arXiv:0804.2509.
[75] V. Zauner-Stauber, L. Vanderstraeten, M. T. Fishman, F. Verstraete, and J. Haegeman, Phys. Rev. B **97**, 045145 (2018).
[76] S. R. White and I. Affleck, Phys. Rev. B **77**, 134437 (2008).
[77] A. K. Bera, B. Lake, F. H. L. Essler, L. Vanderstraeten, C. Hubig, U. Schollwöck, A. T. M. N. Islam, A. Schneidewind, and D. L. Quintero-Castro, Phys. Rev. B **96**, 054423 (2017).
[78] D. Macdougal, S. Williams, D. Prabhakaran, R. I. Bewley, D. J. Voneshen, and R. Coldea, Phys. Rev. B **102**, 064421 (2020).
[79] J. Willsher, H.-K. Jin, and J. Knolle, Phys. Rev. B **107**, 064425 (2023).
[80] F. Ferrari, A. Parola, and F. Becca, Phys. Rev. B **103**, 195140 (2021).
[81] F. Ferrari and F. Becca (private communication).
[82] E. Dupuis, M. B. Paranjape, and W. Witczak-Krempa, Phys. Rev. B **100**, 094443 (2019).
[83] N. E. Sherman, M. Dupont, and J. E. Moore, Phys. Rev. B **107**, 165146 (2023).